Noname manuscript No.
(will be inserted by the editor)

The transition of a line plume to round plume

Nigel B. Kaye · Dylan M. Robinson · Romana Akhter · Md Safwan Ahsanullah · Ta'Jon A. Jordan · Oscar E. Martinez

Received: DD Month YEAR / Accepted: DD Month YEAR

Abstract Buoyant turbulent plumes are often categorized by their geometry and described as either round plumes, issuing from a point source, or line/planar plumes, issuing from an elongated source. As line plumes rise above their source they get thicker (normal to the source axis) and, far from the source, they will no longer be planar but more resemble a round plume. However, the vast majority of experimental measurements of line plumes focus on the near source region, where they are still planar and the flow is two-dimensional. Further, these experiments constrain the ends of the plume with barriers to prevent entrainment through the ends of the plume and maintain a two-dimensional flow. Herein, results are presented from a series of experiments that were conducted to measure the transition of an unconstrained line plume into a round plume. A model is presented that allows the calculation of the entrainment into a plume of arbitrary cross sectional shape in terms of the hydraulic radius of the plume defined as the cross-sectional area divided by the perimeter over which entrainment is occurring. This formulation, along with a smooth transition function that changes both the geometry and entrainment coefficient, is used to make predictions of the front position over time for a line plume in a filling box. The model was run for different values of the nozzle width to box height ratio. Results of the model were compared to the experimental front position measurements and show that an unconstrained line plume will transition to a round plume at a height equal to approximately three times the source width. This is consistent with the idea that the line plume will transition when its thickness is similar in magnitude to its nozzle width.

Keywords Line plume · Round plume · Entrainment · Filling Box

N. B. Kaye
Clemson University
E-mail: nbkaye@clemson.edu

Abbreviations

α	Entrainment coefficient (-)
α_L	Entrainment coefficient for a line plume (-)
$\alpha_{L.G}$	Entrainment coefficient for a line plume with Gaussian velocity profile (-)
α_R	Entrainment coefficient for a round plume (-)
$\Delta\rho$	density difference between the plume and ambient fluid (kg/m^3)
η	non-dimensional first front height (-)
Γ_T	Flux balance parameter at the transition height (-)
λ	non-dimensional plume transition height (-)
ϕ	non-dimensional transition distance (-)
ψ	ratio of the round plume to line plume filling box time (-)
ρ	plume fluid density (kg/m^3)
ρ_0	ambient density (kg/m^3)
τ	non-dimensional time (-)
$\forall$	Tank volume (m^3)
ζ_T	plume transition height scaled on the tank height (-)
b	plume radius or half width (m)
f	buoyancy flux per unit width (m^3/s^3)
g	gravitational acceleration (m/s^2)
g'	reduced gravity m/s^2)
h	height of the first front (m)
m	momentum flux per unit width (m^3/s^2)
q	flow rate per unit width (m^2/s)
u	top hat vertical velocity (m/s)
z	vertical coordinate measured from the plume source (m)
z^*	non-dimensional height (-)
z_T	plume transition height (m)
z_v	virtual origin height (m)
A	Plume cross sectional area (m^2)
A_T	Tank cross sectional area (m^2)
C_L	Line plume flow rate coefficient (-)
C_R	round plume flow rate coefficient (-)
F	buoyancy flux (M^4/s^3)
F_B	buoyancy force (N)
H	Tank height (m)
M	momentum flux (m^4/s^3)
P	Entraining perimeter (m)
Q	volume flux (m^3/s)
Q^*	non-dimensional volume flux (-)
R	Hydraulic Radius (m)
R_T	equivalent radius of tank (m)
R_L	line plume hydraulic radius (m)
R_R	round plume hydraulic radius (m)
S.G.	plume fluid specific gravity (-)
T_{fill}	filling box time for a line plume (s)
W	line plume source width (m)

1 Introduction

Turbulent Line plumes, also known as planar plumes, are ubiquitous in environmental flows. Examples include the thermal plume above the flame front of a wildfire (Albini (1996)), leads formed below ice sheets (Ching et al. (1996)), ocean outflow dispersion (Roberts (1979)), and spill plumes from compartment fires (Thomas et al. (1998)). As a result, there is an extensive literature on the behavior of line plumes in different environments. This includes line plume breakdown in a turbulent environment (Ching et al. (1995)), the interaction of multiple line plumes (Ching et al. (1996)), line plumes in confined regions (Baines and Turner (1969); Akhter and Kaye (2020)), line plumes in ventilated spaces (Linden et al. (1990)), line plumes in stratified (Ma et al. (2017)) and rotating environments (Bush and Woods (1999); Fernando and Ching (1993)), and sub-glacial discharge plumes (Jackson et al. (2017)).

Early work on line plumes by Lee and Emmons (1961) built on the entrainment model of Morton et al. (1956) to developed equations for the flow rate per unit width of a line plume. The model was used to predict the behaviour of plumes from 'neutral' sources (pure line plumes), 'restrained' sources (lazy plumes), and 'impelled' sources (forced plumes). A series of experiments were run to measure the plume temperature and was compared to the model to establish an estimate of the entrainment coefficient of $\alpha_{L.G} = 0.16$ for Gaussian velocity profiles. The experiments were set up with vertical end plates to prevent entrainment into the plume from the ends and ensure that the flow was two dimensional.

The entrainment assumption and momentum equation can be used to form equations for the fluxes per unit width of volume ($q = 2bu$) and momentum ($m = 2bu^2$) leading to

$$\frac{dq}{dz} = 2\alpha_L \frac{m}{q} \tag{1}$$

and

$$\frac{dm}{dz} = \frac{qf}{m} \tag{2}$$

where α_L is the top-hat entrainment coefficient for a line plume and f is the buoyancy flux per unit width. For an ideal source of pure buoyancy the solution to (1) and (2) results in a prediction for volume flux per unit width of

$$q = C_L f^{1/3} z \tag{3}$$

where $C_L = (2\alpha_L)^{2/3}$. The plume half width is given by

$$b = \alpha_L z. \tag{4}$$

Kotsovinos & List ran experiments to measure the integral properties (Kotsovinos and List (1977)) and turbulent properties (Kotsovinos (1977)) of two-dimensional line plumes. Experiments were run using warm water for the buoyant fluid. They established mean and turbulent properties including distribution of tracer fluxes between the mean and turbulent flow. As with Lee and Emmons (1961), the experimental setup had solid walls at each end of the plume to prevent entrainment through the ends and to ensure a mean two-dimensional flow.

There have been numerous other experimental studies of the behaviour of line plumes that have refined measurements of the entrainment coefficient (Ramaprian and Chandrasekhara (1989); Paillat and Kaminski (2014); Parker et al. (2019)). See Parker et al. (2019) for a review of experimental measurements. While there are many different approaches to forming line plumes and making measurements used in the studies cited above one consistent element is the use of end walls normal to the plume source nozzle. This has two effects. First, it prevents entrainment of ambient fluid through the ends of the plume. Second, it prevents the the plume growing in those directions and ensures a purely two-dimensional flow during the experiments.

If the end walls are removed there is potential for entrainment through the ends and, given a large enough vertical distance to develop, the plume will eventually cease to be long (in the direction of the nozzle axis) and thin (normal to that axis) and will ultimately transition into a round plume. To the best of the authors' knowledge, the only experimental study that has looked at line sources without end constraints is by Hu et al. (2017). They studied the flame height from a line burner for different configurations of flow constraint. They measured the flame height for a line burner enclosed between parallel walls for different wall spacing and wall orientation. When the walls were parallel to the long axis of the nozzle the flame height increased as the walls were moved closer to the flame. This was attributed to the reduced entrainment of oxygen into the flame due to the constraining side walls. When the walls were placed normal to the long axis of the nozzle, the observed flame height was constant regardless of the separation of the walls from each end of the nozzle (see Figure 1). This implies that, at least for the parameter range tested, end entrainment may not be that significant. The images in Figure 1 not only show that the flame height is independent of the end constraints, but that sides of the plume are relatively vertical implying that any entrainment through the ends of the line plume had a minimal impact on the flame width. Hu et al. (2017) did not address the transition in behavior from a line fire to a round fire.

The problem of the transition of a line plume into a round plume has received very little attention though it has practical applications. For example, the behavior of displacement ventilation systems in enclosures with finite length line sources of heat will behave differently depending on the ratio of the height of the enclosure to the length of the source. For example, consider an HVAC system floor level heating vent with a length of $W = 50$ cm in a room with a $H = 2.5$ m ceiling (both typical of domestic systems). If it were a line plume it would have a thickness of $2b = 2\alpha_L 2.5m \approx 80$ cm when it reaches the ceiling (using a typical value of $\alpha_L = 0.155$, see Lee and Chu (2003)). The ventilation rate and the stratification that develops in plume driven displacement ventilation system depends on the plume geometry (Linden et al. (1990)). In this case there it is quite likely that the line plume would transition to a round plume before reaching the ceiling. It is important to know at what height the transition from line plume to round plume behavior occurs in this

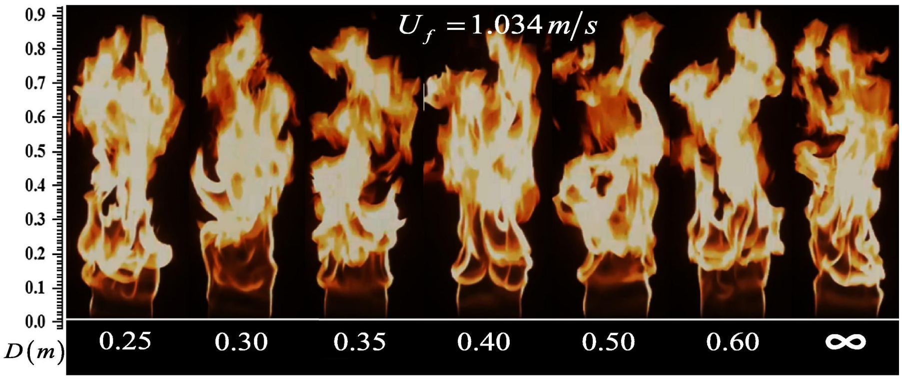

Fig. 1 Instantaneous images of flames issuing from a 2 mm by 145 mm propane source with end walls normal to the long axis of the source. Images are shown for different spacing between the end walls (D). From Hu et al. (2017), used with permission.

case in order to be able to correctly predict the ventilation flow rate and room stratification.

Two studies have addressed this issue. Bejan et al. (2014) argued that plumes and jets will adjust their geometry to maximize mixing and suggested that this will result in a minimization of the mean vertical velocity with height and that the transition height z_T will scale on the source width. However, no experimental results were presented. Thomas (1987) looked at smoke spill plumes that are formed by smoke flowing over the underside of a ceiling and then out an elongated opening such as a window or the underside of a balcony. They modeled the plume as a line plume up to a certain height and then as a round plume. The round plume that forms above the transition can be modelled as a round plume with a virtual origin offset. However, this paper also lacks experimental data and a clear value for the transition height or the resulting virtual origin. Both these models are discussed in more detail below.

While there is a dearth of literature on line plumes transitioning to round plumes, there have been studies of other plume flow transitions. In particular, there is a considerable literature on the merger of round plumes to form either another round plume (Baines (1983); Kaye and Linden (2004); Rooney (2016); Li and Flynn (2020b)) or a line plume (Rooney (2015); Li and Flynn (2020a)). Kaye and Linden (2004) assumed that the plumes acted as separate plumes up to the height at which they merged and then calculated the virtual origin of the resulting single plume assuming that its shape was circular. Their experimental flow rate measurements showed that this approach gave a reasonable estimate of the virtual origin of the far field plume and that the transition occurred over a finite but small distance. the finite but short transition from separate to merged plumes was also seen in the experiments of Baines (1983).

An alternate approach for modeling was presented by Rooney (2016) for the merger of two round plumes into a single round plume and Rooney (2015) for the merger of a row of round plumes into a line plume. They calculated contours of constant velocity potential in a horizontal plane for a vertical line sink to get the plume shape and coupled this model with a generalized entrainment model to solve for the flow rate as a function of height. This approach was extended by Li and Flynn (2020a) for parallel rows of round plume sources. The advantage of this approach is that the model does not assume a shape for the horizontal cross section of the plume but rather calculates it based on the contours of constant velocity.

Despite all the research discussed above, there is still an open question regarding the height at which a line plume will transition to a round plume. Further, there are no models for how the plume behaves in the vicinity of this transition. The goal of this paper is to address these gaps in the literature through model development validated by a series of filling box experiments that capture the line plume to round plume transition behaviour. The remainder of the paper is structured as follows. A model is presented for entrainment into a plume of arbitrary cross sectional geometry in §2 along with a discussion of transition models the transition height, and the first front movement of a line-to-round plume in a filling box. The experimental setup is described in §3 followed by experimental results in §4. The results are discussed and conclusions drawn in §5.

2 Model development

We consider a buoyant plume with a general geometry and top-hat profiles that entrains ambient fluid. We define the fluxes of volume, momentum, and buoyancy as

$$Q = uA, \quad M = u^2 A, \quad \text{and} \quad F = g' Q \tag{5}$$

where A is the flow cross sectional area and u is the mean velocity. The reduced gravity g' is defined as

$$g' = g \frac{\Delta\rho}{\rho_0} \tag{6}$$

where ρ_0 is the ambient density and $\Delta\rho$ is the density difference between the mean density in the plume and the ambient density. The density difference is taken to be small such that the Boussinesq approximation is valid.

2.1 Entrainment model for generalized plume geometry

In general conservation of volume for a control volume of height dz can be written as

$$Q + dQ = Q + \alpha u P dz \tag{7}$$

where P is the perimeter over which entrainment occurs and α is the top hat entrainment coefficient for a particular geometry plume. See Figure 2. Writing $u = Q/A$ leads to

$$\frac{dQ}{dz} = \alpha \frac{Q}{R} \tag{8}$$

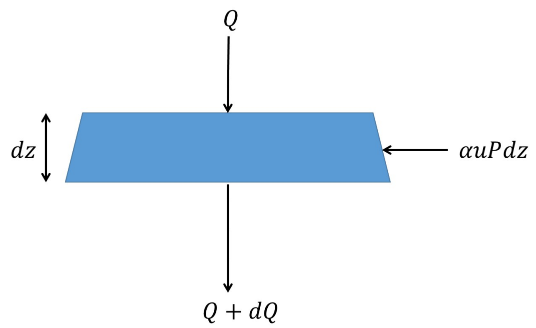

Fig. 2 Control volume showing inflows and outflows from a plume section of height dz.

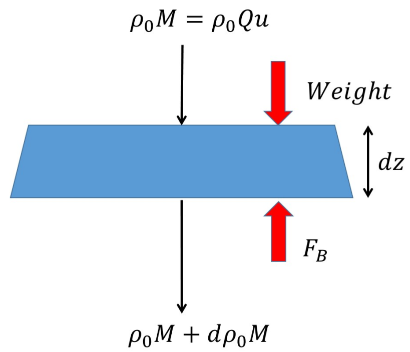

Fig. 3 Force and momentum diagram showing the forces acting on the plume and the resulting change in momentum.

where

$$R = \frac{A}{P} \tag{9}$$

is the hydraulic radius of the plume based on the perimeter over which entrainment occurs.

Making the standard assumption that the plume is relatively long and thin and that the pressure can be assumed to be hydrostatic, the linear momentum equation can be written as

$$\rho_0 g A dz - \rho g A dz = \rho_0 dM. \tag{10}$$

The first term on the left hand side is the buoyancy force and the second term is the weight of plume fluid in the control volume. See Figure 3. This simplifies to

$$\frac{dM}{dz} = g' A = \frac{g' Q^2}{M} = \frac{QF}{M}. \tag{11}$$

Equations (8) and (11) reduce to the standard plume flux equations for a line source or point source by substituting the appropriate geometry for the hydraulic radius and using the appropriate entrainment coefficient (α_R or α_L for round and line plumes respectively).

For a point source $A = \pi b^2$ and $P = 2\pi b$ giving $R_R = b/2$ and $u = M/Q$ leading to

$$\frac{dQ}{dz} = 2\alpha_R \sqrt{\pi M}. \tag{12}$$

For a line plume with no entrainment through the ends $P = 2W$ and $A = 2bW$ leading to

$$\frac{dQ}{dz} = 2\alpha_L \frac{M}{Q}. \tag{13}$$

In both cases the momentum equation is (11).

Writing the plume equations in a general form as (8) and (11) allows the fluxes to be calculated by numerical integration provided the hydraulic radius can be easily calculated from the fluxes (Q and M) at each step. For a round plume $R_R = Q/2\sqrt{\pi M}$ and for a line plume that is not entraining at the ends $R_L = Q^2/2WM$. This is more complex for other geometries, such as for ellipsoidal bent over plumes or line plumes where there is significant entrainment at the ends.

If entrainment through the end of the plume is included in the model then there is a need for a model for the shape of the plume ends. Visual observation from the experiments described below indicates that near the source the plume maintains a constant width equal to that of the nozzle width even in the absence of end walls. Therefore, a first order approximation would be that the perimeter would be $P = 2(W + 2b)$ where b is the plume half thickness. This can be calculated from the plume fluxes by calculating the plume velocity ($u = M/Q$), then the area ($A = Q/u$), and finally the half width ($b = A/2W$).

2.2 Plume Transition

There are a number of possible options for modeling the transition from a line to a round plume. However, regardless of the approach, there are two main questions that need to be answered: (1) at what height does the transition occur and (2) over what vertical distance does the plume transition from a pure line plume to a pure round plume. While it is not known a priori what the values of the transition height and transition length are, it is possible to get estimates of these values as discussed below.

One simple model would be to assume that the transition is instantaneous at some height (z_T) and matching the plume volume fluxes at that height. This is the approach discussed in Thomas (1987) though there was no explicit prediction of the transition height. Measuring height from the line plume source (assumed ideal) the volume flux for a line plume can be written as

$$Q_L = C_L F^{1/3} W^{2/3} z \quad \text{for} \quad z \le z_T. \tag{14}$$

where $C_L = (2\alpha_L)^{2/3}$. Matching the round plume flow rate at z_T requires a virtual origin offset leading to the round plume volume flux being given by

$$Q_R = C_R F^{1/3} (z + z_v)^{5/3} \quad \text{for} \quad z \ge z_T \tag{15}$$

where $C_R = \pi^{2/3} \left(\frac{5}{8}\right)^{1/3} \left(\frac{6}{5}\right)^{5/3} \alpha_R^{4/3}$.

Dimensional analysis requires that $z_T = z_T(W)$ and, therefore, that $z_T = \lambda W$ where λ is an (unknown) constant. The flow rates in the line and round plume are the same at $z = z_T$. Therefore we can solve for the virtual origin to give

$$\frac{z_v}{W} = \left(\lambda \frac{C_L}{C_R}\right)^{3/5} - \lambda. \tag{16}$$

However, this approach leads to a discontinuity in the momentum flux as it assumes that the round plume that forms at the transition height is a balanced pure plume. It is shown later that this is not the case.

An alternative approach is to solve the plume flux equations (8) and (11) with an empirical function that transitions from 0 to 1 over some range of z centered on z_T. For illustration we use the logistic function

$$L\left(\frac{z}{W}\right) = \frac{1}{1 + e^{\phi\left(\lambda - \frac{z}{W}\right)}}. \tag{17}$$

The logistic function is $L = 0$ for small z/W, $L = 1$ for large z/W and $L = 0.5$ when $z/W = \lambda$. The larger the value of ϕ the shorter the distance over which the transition occurs.

For the transition of a line plume to a round plume both the geometry and entrainment coefficient change. Therefore the volume flux equation becomes

$$\frac{dQ}{dz} = Q\left(\frac{\alpha_L}{R_L} + L\left(\frac{z}{W}\right)\left(\frac{\alpha_R}{R_R} - \frac{\alpha_L}{R_L}\right)\right). \tag{18}$$

The advantage of this approach is that there is no shape assumed during the transition. Instead of modeling the flow as, for example, an ellipse with major and minor radii that adjust with height, the shape is characterized only in terms of its hydraulic radius (R) that is a weighted average of the hydraulic radii of the equivalent round and line plumes. This approach is similar to the velocity potential model of Rooney (2015) in that the plume flux equations treat the area generically. That is the geometry is not built into the equations. However, the model of Rooney (2015) then couples this with a potential flow model that calculates the shape of, in their case, the merging round plumes. In the approach described herein the shape is not calculated. Instead a characteristic length of the shape, the hydraulic radius, is assumed to be a weighted average of the hydraulic radii of the equivalent round and line plumes. This approach sacrifices the calculation of the plume shape for computational simplicity.

The solution to the model found by numerical integration of the coupled plume flux equations (11) and (18). The integration was done using MATLAB built in functions for integrating ODEs. The hydraulic radius at each height was calculated using the following steps. First, the flow velocity was calculated based on the momentum and volume fluxes with $u = M/Q$. The flow cross-sectional area was then calculated based on the velocity and volume flux ($A = Q/u$). Finally, the area was used to calculate the characteristic thickness of

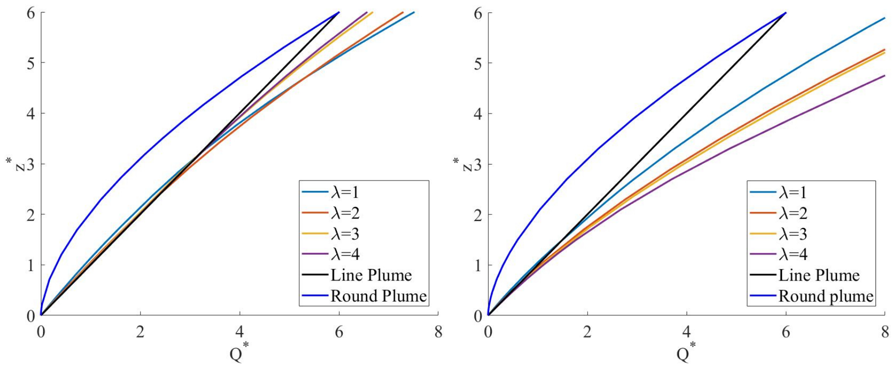

Fig. 4 Plots of normalized flow rate for different values of λ and $\phi = 1$ when (left) end entrainment is turned off and (right) end entrainment is turned on. In both figures the black line is for a pure line plume with no end entrainment.

the plume for each idealized shape. For a round plume the radius is given by $b = \sqrt{A/\pi}$ and the hydraulic radius is $R_R = A/P = b/2$. For a line plume the plume half thickness is given by $b = A/2W$. The entraining perimeter is then $P = 2W$ if end entrainment is not included and $P = 2W + 4b$ if end entrainment is included. The hydraulic radius is then given by $R_L = A/P$. We note that, when end entrainment is included in the model, the entrainment coefficient used is the same as for a pure line plume. This value was used as a first order approximation given the lack of experimental measurements of this parameter.

Plots are presented of volume flow rate against height for different combinations of λ and ϕ in Figures 4 and 5. In each plot the volume flow rate is normalised by the flow rate in a pure line plume at the vertical distance of one nozzle width above the origin and is denoted by

$$Q^* = \frac{Q}{C_L F_0^{1/3} W^{5/3}}. \tag{19}$$

Vertical distance is normalized by the nozzle width and is denoted by

$$z^* = \frac{z}{W}. \tag{20}$$

Figure 4 shows the flow rate as a function of height for $\phi = 1$ and different values of λ. Figure 4(a) is for the model with no entrainment through the ends of the plume. The model behaves as one might expect. The lower the value of λ the earlier the line diverges from the line plume eventually having a larger flow rate for a given height. It is interesting to note that for low heights and $\lambda = 1$ the flow rate is actually less than that of a pure line plume because the transition occurs before the vertical gradient of volume flux is higher in the line plume compared to the round plume. This point is discussed in §2.3. Finally, for $z^* < 3$ there is very little difference in the flow rate for the range of λ considered. This suggests that for filling box experiments run with a depth

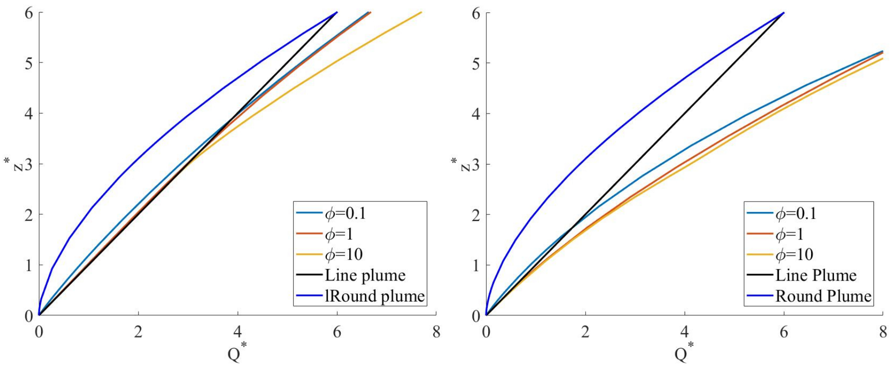

Fig. 5 Plots of the normalized plume flow rate for different ϕ and $\lambda = 3$ when (left) the end entrainment is turned off and (right) the end entrainment is turned on.

$H < 3W$ will likely not allow for a clear identification of the transition height based on the first front movement.

When end entrainment is included in the model the order is reversed (Figure 4b). The end entrainment results in the entraining perimeter of the line plume growing more rapidly than the round plume such that, in the far field, the flow rate is larger for plumes that have a larger transition height (larger λ).

For all the transitions shown in Figure 4, the transition length parameter was kept at $\phi = 1$. To see the impact of ϕ on the transition behaviour the normalized flow rate is plotted for $\lambda = 3$ for different values of ϕ in Figure 5. When there is no end entrainment (Figure 5a) there is little distinction between the flow rates for the lowest two values of $\phi = 0.1$ and 1. Only the sharper transition ($\phi = 10$) shows a clearly larger flow rate. When end entrainment is included in the model there is very little difference in the far field flow rates (Figure 5b) This is because the additional entraining perimeter at the ends mimics the growth in perimeter with height of a round plume leading to somewhat similar behavior for the three values of ϕ plotted.

2.3 Transition heights

It is not known a priori what the values of the transition height and transition length are, however, it is possible to get estimates of these values. There are various approaches to modeling the height at which the plume will transition from a line plume to a round plume. In all cases the problem reduces to finding a constant λ where the transition height is $z_T = \lambda W$.

Bejan et al. (2014) argues that at all heights the geometry will be such as to maximize the mixing. This was interpreted as meaning that at all heights the mixing would be such as to produce the lowest mean velocity (maximum flow rate for a given momentum flux). For a round plume the velocity decays with height whereas a line plume is a constant velocity flow. The supplementary material for Bejan et al. (2014) provides empirical equations for the velocity of a round and line plume. Solving for the height at which the velocities for each shape plume match, under the assumption that they have the same source height, leads to $\lambda = 3.1$.

However, there is an implicit assumption that the momentum flux is constant which is valid for turbulent jets (also considered by Bejan et al. (2014)) but not for turbulent plumes. The entrainment hypothesis says that the rate of increase of volume flux with height is the product of the plume velocity u, the entrainment coefficient α, and the perimeter over which entrainment is occurring P. That is, $dQ/dz = \alpha u P$. Therefore, the hypothesis that mixing is maximized (Bejan et al. (2014)) should be stated in terms of the vertical gradient of volume flux. That is, the transition should occur when

$$\frac{dQ}{dz}_{line} = \frac{dQ}{dz}_{round}. \tag{21}$$

Below the transition the plume will behave as a line plume such that the velocity at any height ($z < z_T$) is

$$u = Q/A = (2\alpha_L)^{-1/3} F^{1/3} W^{-1/3} \tag{22}$$

and the momentum flux is given by

$$M = Qu = (2\alpha_L)^{1/3} F^{2/3} W^{1/3} z. \tag{23}$$

Assuming that there is no entrainment through the ends of the plume then equating the volume flow rate gradients (21) leads to

$$2\alpha_L u W = 2\alpha_R \sqrt{\pi M}. \tag{24}$$

Substituting (22) and (23) into (24) leads to

$$2\alpha_L (2\alpha_L)^{-1/3} F^{1/3} W^{-1/3} W = 2\alpha_R \sqrt{\pi (2\alpha_L)^{1/3} F^{2/3} W^{1/3} z} \tag{25}$$

and a prediction of $\lambda = 1.9$. The line plume momentum flux is used in the RHS of (25) as the momentum flux of the flow at this transition height is that generated by the line plume from the physical source to this transition height. This approach requires a second assumption. When the volume flux gradients are matched it is assumed that the comparison is between a pure line plume and a pure round plume both with sources at the same height. However, when the plume transitions from a line to a round plume, it is unlikely that the resulting round plume will have a virtual origin at the height of the line plume origin. Therefore, this approach requires the use of a virtual origin offset for the round plume that is not known a priori.

An alternate approach is to assume that a line plume will transition to a round plume when the aspect ratio of the plume ($2b/W$) is of $O(1)$. That is, when the plume source width W is no longer significantly greater than the thickness of the plume $2b$ where b is the plume half width normal to the axis of the source. For a line plume $b = \alpha_L z$ such that the transition will occur when $2b = 2\alpha_L z \sim W$ This leads to $\lambda \sim 1/2\alpha_L \approx 3.2$. This approach has the advantage of not requiring any assumption about the resulting round plume and is purely based on the shape of the line plume that can be established from existing models.

2.4 filling box model first front movement

The goal of this study is to establish the height above the source at which a line plume will transition to a round plume. This is to be done through analysis of the first front movement in a series of filling box experiments (Baines and Turner (1969)). The position (h) of the first front in a filling box can be calculated by applying conservation of volume to the buoyant layer behind the first first. In general this is given by

$$\frac{dh}{dt} = \frac{1}{A_T} Q_{plume}(z = h) \tag{26}$$

where A_T is the cross sectional area of the tank/box and the distance h is the measured from the plume source.

For a line plume, conservation of volume of the buoyant layer leads to

$$\frac{dh}{dt} = -\frac{C_L W^{2/3} F^{1/3} h}{A_T}. \tag{27}$$

This can be integrated from $z = H$ at $t = 0$ to give

$$\frac{h}{H} = \eta = e^{-\tau} \tag{28}$$

where

$$\tau = \frac{t}{T_{fill}} \tag{29}$$

and

$$T_{fill} = \frac{A_T H}{C_L W^{2/3} F^{1/3} H} = \frac{\forall}{Q_L(z = H)} \tag{30}$$

is the filling time defined as the tank volume divided by the plume flow rate at the base of the tank. The symbol $\forall$ is used to denote the volume of the box.

The full model (equations 11, 18, and 26) can be solved numerically. However, the analytic result for the simple virtual origin offset model is presented for illustration. For a line plume that transitions to a round plume at $z = z_T$ (equations 15 and 16), conservation of volume for $z > z_T$ leads to

$$\frac{dh}{dt} = -\frac{C_R F^{1/3} (h + z_v)^{5/3}}{A_T}. \tag{31}$$

Again integrating from $h = H$ at $t = 0$ leads to

$$\frac{\eta + \zeta_v}{1 + \zeta_v} = \left(1 + \frac{2 C_R F^{1/3} H^{5/3}}{3\forall} (1 + \zeta_v)^{2/3} t\right)^{-3/2} \tag{32}$$

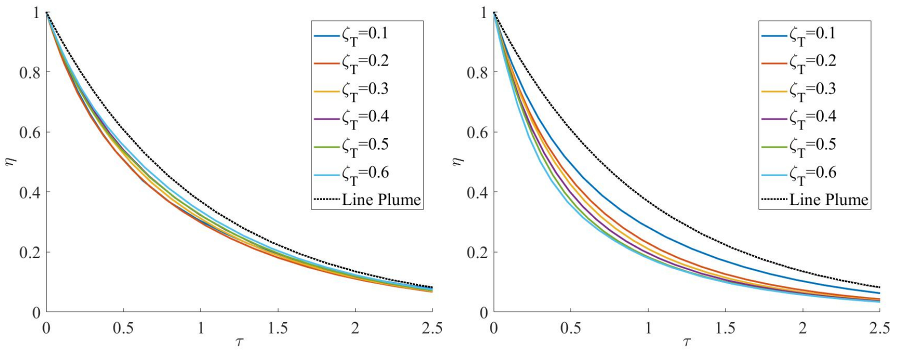

Fig. 6 Plots of the front position for a filling box experiment for different ζ_T with $W/H = 0.1$ and $\phi = 2$. (left) End entrainment turned off and (right) end entrainment turned on.

where $\zeta_v = z_v/H$. This can be re-written in non-dimensional form as

$$\eta + \zeta_v = (1 + \zeta_v)\left(1 + \frac{\psi\tau}{(1 + \zeta_v)^{2/3}}\right)^{-3/2} \tag{33}$$

where

$$\psi = \frac{2C_R}{3C_L}\left(\frac{H}{W}\right)^{2/3} \tag{34}$$

is proportional to the ratio of the line plume to round plume filling box times.

Plots of the front position (η) for the full model are shown in Figure 6 for a plume with a source width $W = 0.1H$ and different λ. The line's labels show the normalized height at which the plume transitions from line to round ($\zeta_T = \lambda W/H$). When end entrainment is turned off (Figure 6a) the flow rate in the plume is smaller prior to the transition compared to when end entrainment is included. Therefore, the further from the source the transition occurs, the slower the front movement will be as the reduced entrainment occurs over a greater height, though the differences are quite small. This is consistent with Figure 4(a) as the flow rate at a given height is larger for lower λ. Conversely, when end entrainment is turned on (Figure 6b) the opposite is true and the differences in front position over time are slightly larger between the different values of λ.

However, the non-dimensional front position is also a function of the nozzle width to box height ratio. In fact, more generally, the first front is

$$\eta = \eta(\tau, \lambda, W/H, \phi) \tag{35}$$

However, Figure 6 shows only $W/H = 0.1$. When λ is held constant and W/H is varied the picture changes. This is shown in Figure 7 for $\lambda = 3$ and $\phi = 2$. In this case the narrower the nozzle the faster the front descends as the plume transitions to a higher flow rate round plume closer to the nozzle. When end mixing is included in the model, the order of the lines remains the same but the front descends more rapidly due to the additional end entrainment.

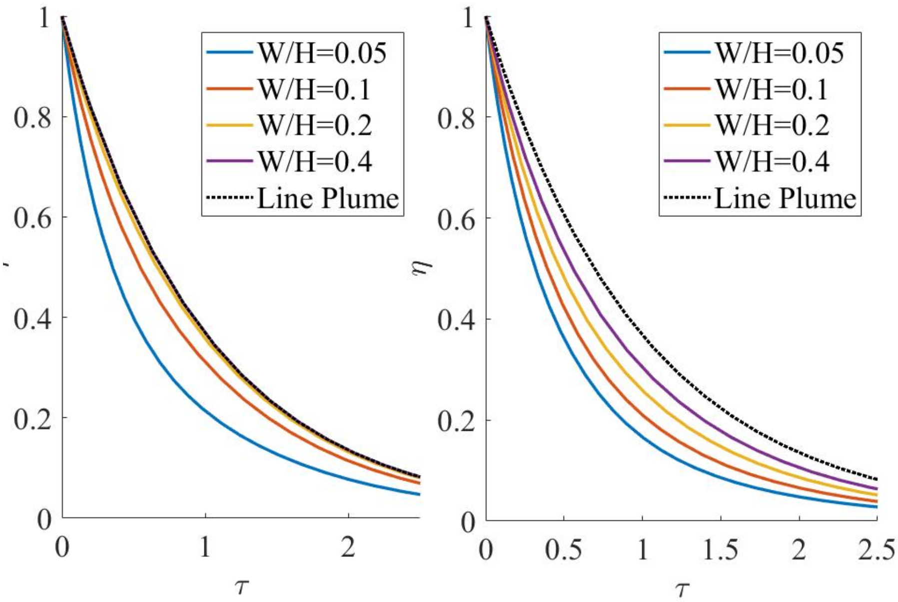

Fig. 7 Plots of the front position for a filling box experiment for different W/H with $\lambda = 3$ and $\phi = 2$. (left) End entrainment turned off and (right) end entrainment turned on.

The impact of ϕ on the front position is shown in Figure 8 along with the overly simplified model of an instantaneous transition from pure line to pure round plume (equations 14-16 and 33-34). When there is no end entrainment the difference between the line and round plume entraining perimeter is larger compared to when end entrainment is turned on. Therefore, the distance over which the transition occurs has a greater impact on the flow rate and resulting first front position.

It is interesting to note that, even for large ϕ, that is very rapid transition from line to round plume, the front position moves more slowly than the simplest model that assumes a sharp transition from a pure line plume to a pure round plume. This suggests that, at the point of the transition, the resulting round plume has a virtual origin that is closer to the transition point than the virtual origin for a pure plume calculated using (16) as the slower front movement means lower plume flow rate and less distance from the virtual origin. This in turn implies that the round plume is forced at the transition point (Morton and Middleton (1973); Hunt and Kaye (2005)). This can be verified by looking at the round plume flux balance parameter Γ at the transition height z_T. The flux balance parameter is $\Gamma = 1$ if the plume fluxes are consistent with the similarity solution for a round plume, a so called pure plume. If $\Gamma > 1$ there is a relative deficit of momentum compared to a pure plume with the same buoyancy and volume fluxes. Likewise, if $\Gamma < 1$ there is

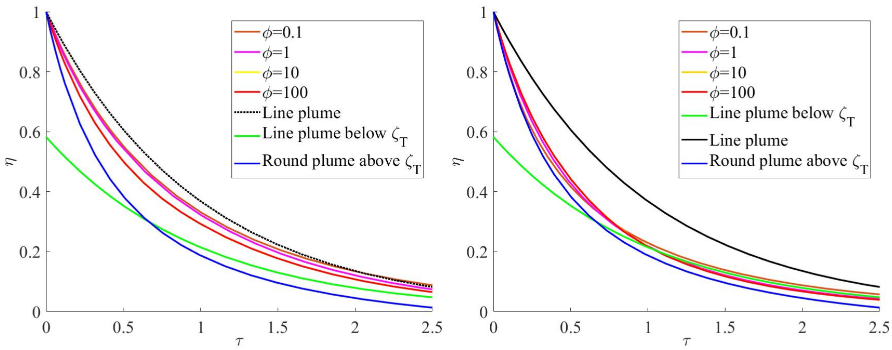

Fig. 8 Plots of the front position for a filling box experiment for different ϕ with $W/H = 0.1$ and $\lambda = 3$. Also shown is the predicted front position in which the plume is assumed to be a pure line plume below the merge height (14) and a pure round plume above the merge height (15). (left) End entrainment turned off and (right) end entrainment turned on.

a relative excess of momentum compared to a pure plume. The value of Γ at the transition height can be calculated by substituting the line plume fluxes of volume Q, (14), buoyancy (F_0) and momentum, given by

$$M = \frac{Q^2}{A} = \frac{C_L^2 F_0^{2/3} W^{4/3} z^2}{2\alpha_L z W} = C_L^{1/2} F_0^{2/3} W^{1/3} z, \tag{36}$$

into the round plume equation for Γ. At the transition height $z_T = \lambda W$ the round plume flux balance parameter

$$\Gamma_T = \frac{5}{16\alpha_R\sqrt{\pi}} \frac{Q^2 F}{M^{5/2}} = \frac{5}{16\alpha_R\sqrt{\pi}} \frac{C_L^2 F_0^{5/3} W^{4/3} z^2}{C_L^{5/4} F_0^{5/3} W^{5/6} z^{5/2}}. \tag{37}$$

Substituting $z = \lambda W$ and values for C_L and α_R leads to

$$\Gamma_T = 0.84\lambda^{-1/2} \tag{38}$$

which is less than 1 for $\lambda > 0.71$. Therefore, provided the transition from a line to a round plume occurs at a distance greater than $z_T = 0.71W$, the resulting round plume will be initially forced. That is, a pure line plume will become a forced round plume due to the change in geometry and resulting similarity solution. For the remainder of the paper we only present results for the entrianment model for the flow rate in the transitioning plume and do not include results from the simplified volume flux matching approach.

While there are many complex interactions between the ratio of the nozzle width to box depth ratio, λ, and ϕ, careful analysis of the front position over time in a filling box with a line source that is narrow compared to the depth of the box should show both line and round plume behaviours. Therefore, such an experiment would elucidate the transition behaviour for a line plume developing into a round plume. The experiments described below are designed to provide such an empirical estimate of the transition height $z_T = \lambda W$.

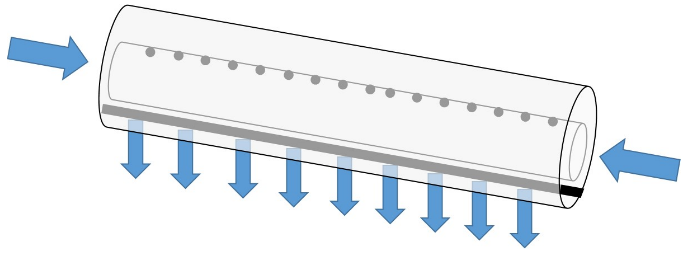

Fig. 9 Schematic diagram of the line plume nozzle showing the fluid supply to the perforated inner tube and the outflow from the slot in the outer tube.

3 Experimental setup

A series of filling box experiments were run to establish the height at which the line plume transitioned into a round plume. Experiments were run for a range of plume source widths and buoyancy fluxes. The experiments were run in a 1.19 m by 1.22 m cross sectional area tank that was 0.57 m deep. The tank had two glass walls for flow visualization. In all cases the width of the line source was less than the width of the tank such that the side walls of the tank did not inhibit flow into the plume. The largest nozzle was 19.4 cm wide giving a minimum tank width to source width ratio of over 6:1.

The line plume was formed using a double tube nozzle design. The outer tube had a 3 mm slit along the base of the tube where the dense salt water was released into the fresh water of the tank. The inner tube had perforations along the top of the tube. Salt water was supplied through both ends of the inner tube and flowed out of the upward facing perforations. This flooded the outer tube with salt water that then passed out of the slit in the outer tube. Visual inspection of the outflow indicated that it was effectively uniform along the full length of the nozzle slit. A schematic diagram of the nozzle can be seen in Figure 9.

Dyed salt water was supplied to the nozzle from a constant head tank placed well above the height of the free surface in the visualization tank. The salt water flowed out of the constant head tank, through a rotameter flow rate meter then into the nozzle. The flow rate meter was equipped with a needle valve for fine control of the flow rate. A second ball valve was fitted just upstream of where the tubing split to feed either end of the nozzle inner tube. The ball valve was used during the experimental set up to allow bubbles to be flushed from the tubing and to start and stop each experiment rapidly. A schematic diagram of the experimental set up is shown in Figure 10.

The dense salt solution was dyed with red food colouring for flow visualization. The visualization tank was lighted from one side and filmed using a camera on the other side of the tank. The lighting was done using a pair of photographic box lights that provided relatively uniform white light across the sections of the tank either side of the plume. For many of the experiments there was a dark section between the two light boxes that prevented clear vi-

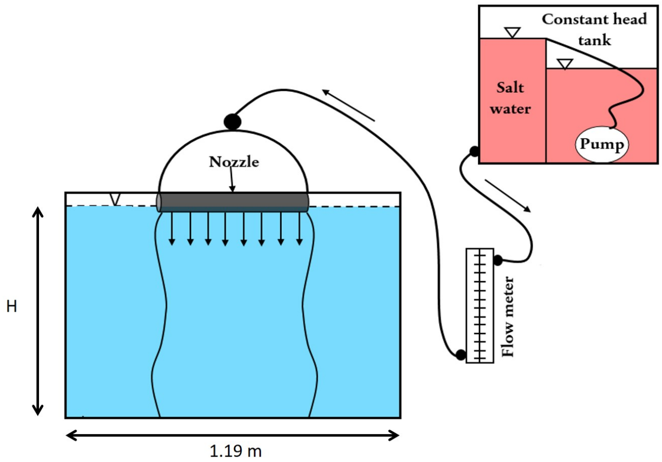

Fig. 10 Schematic diagram of the experimental setup showing the saline supply from the constant head tank, through the rotameter flow rate meter, and into the line source nozzle.

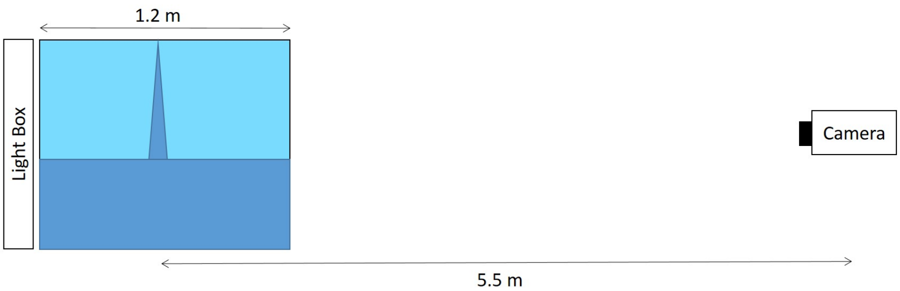

Fig. 11 Schematic diagram of the side view of the visualization setup showing the box lights, the filling box experiment and the distance to the camera used to record the experiments.

sualization of the plume. Two cameras were used during the experiments. The first 3 experiments used a colour camera. The last 3 used a black and white camera. The change in camera was due to equipment availability. The image analysis was the same in each case. A diagram of the visualization set up is shown in Figure 11.

Each experiment was performed using the same technique. The large visualization tank was filled and then allowed to settle for several hours to remove and background motions produced by the filling hose. After that, the nozzle was immersed in the tank and all the bubbles removed. The nozzle was then connected to the feed tube underwater to prevent the introduction of any new air bubbles. The nozzle was then placed in the middle of the tank with its axis normal to the line of sight of the camera such that the width of the plume could be observed. The distance from the nozzle outlet to the tank floor was measured using a tape measure. Once the nozzle had been placed the pump

Table 1 Table of experimental parameters giving the depth from the nozzle to the tank base (H), the nozzle width (W), the source fluid specific gravity (S.G.), the source flow rate (Q) and the nozzle width to water depth ratio (W/H).

Exp.	H (cm)	W (cm)	S.G.	Q (l/min)	W/H
A	52	19.4	1.19	2.2	0.37
B	55	19.4	1.19	1.8	0.35
C	54	10.8	1.1	0.7	0.20
D	49	6.7	1.1	0.6	0.14
E	49	3.8	1.1	0.6	0.078
F	49	2.9	1.1	0.4	0.059

in the constant head tank was turned on and the density of the salt water was measured using a hydrometer. Finally the video recording was started and then the plume flow was started. The experiment was run until the first front in was close to the nozzle. Experiments ranged in time from 20-50 minutes depending on the nozzle width and source buoyancy flux. A summary table showing the parameters for each test is given in Table 1.

As the experimental set up was not in a fully dark room the full dye calibration (Allgayer and Hunt (2012)) was not possible and, therefore, only the front position over time is recorded, and not the stratification below the first front.

4 Experimental results

At the start of each experiment the plume flowed to the bottom of the tank and spread out horizontally. Upon reaching the side walls of the tank the plume fluid flowed up the side walls and then slumped back down forming the stable lower layer. See Figure 12 for a series of images taken from the video of experiment A which exhibited the largest side wall up-welling at the start the experiment. No overturning was observed when the outflow rose up the side walls. This is consistent with stability criteria suggested by Baines and Turner (1969) and the experiments of Kaye and Hunt (2007). Baines and Turner (1969) found that the flow was stable for $H/R_T < 1$ where R_T is the radius of the box. The experiments of Kaye and Hunt (2007) showed that, for a round plume, overturning at the side walls occurs for $H/R_T > 1.5$. For the rectangular cross section tank used herein the equivalent radius is taken to be $R_T = \sqrt{A_T/\pi}$. The largest value used in the experiments presented herein was $H/R_T = 0.8$ leading to no overturning. However, the up-welling and slumping did delay the formation of a stable interface. As such, the front position could only reliably be identified once the the tank was partially full of buoyant fluid.

For the experiments run for this study the Reynolds numbers based on the nozzle slot width were quite small (Re=110-260). There is, therefore, the possibility that the outflow could be laminar. However, the Reynolds numbers for the flow through the perforations on the top of the inner tube were over an order of magnitude larger than this. Further, experiments on round plumes

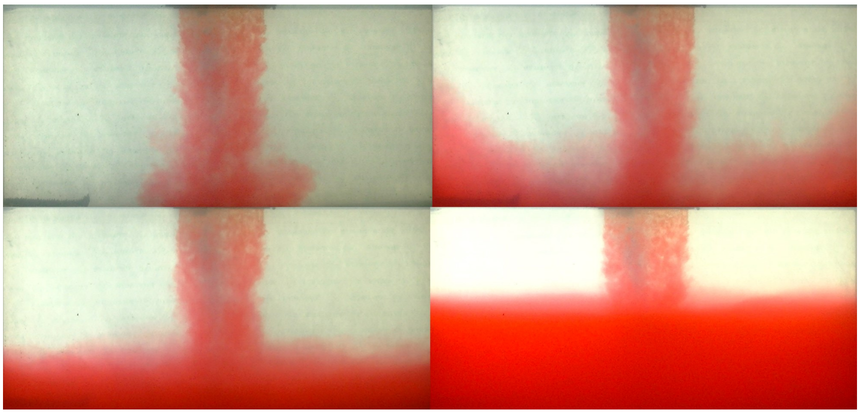

Fig. 12 Series of images of experiment A ($W/H = 0.37$) showing from top left (a) the initial plume descent, (b) the plume outflow rising up the side walls, (c) the dense lower layer formed after the outflow slumps back down, and (d) the sharp density interface at the top of the dense lower layer at later times.

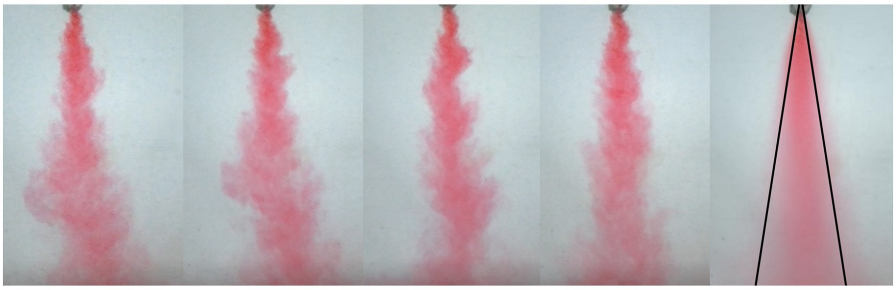

Fig. 13 Series of images of a separate visualization experiment with ($W/H = 0.15$) and a source Reynolds number of $Re = 165$. Images shown are with the line plume source parallel to the line of sight. The images show, from left to right, four instantaneous images of the plume and an image averaged over the first 20 seconds after the plume reached the base of the tank. The black lines represent the predicted plume width for a pure line plume.

found that, if the flow was tripped near the source, a plume will remain turbulent even for Re of order 200 (see Huppert et al. (1986)). Even if the flow was laminar and remained so for a couple of slot widths prior to becoming turbulent, the resulting offset would be of the order of 1% of the experimental test height and could be neglected for the majority of the filling box flow. As a final check, a test was run with the plume nozzle rotated through 90^o so that the camera view was along the long axis of the plume. Images of the plume from this test are shown in Figure 13. Despite the Reynolds number only being 165, there is no clear sign of the flow being laminar as it leaves the nozzle. The final panel in Figure 13 shows a 20 second time average image. While the lighting in the laboratory did not allow for full dye calibration and direct measurement of the plume thickness, the shape shows good qualitative agreement with the black lines that represent the top-hat plume outline for a pure line plume.

Another observation was that the sides of the line plume appeared vertical in the near source region. For the experiment shown in Figure 12, which had the widest nozzle, the sides appear vertical over most of the height with the exception of a slight contraction right at the outlet from the nozzle. This suggests that, at least in the near source region, end entrainment does not alter the width of the plume. This does not mean that its cross section remains approximately rectangular near the source. Experiments that directly measure the plume cross section area and shape would be required to resolve the exact shape, perimeter, and area of the cross-section. These were not possible with the setup available to the authors. However, it is noteworthy that the observation of vertical sides is consistent with the observations of the line flames in the experiments of Hu et al. (2017). The slight necking right at the outlet may be due to the flow of dense fluid along the nozzle at either end of the outlet slot. Care was taken to ensure that the pipe sections on either end of the nozzle slot were blocked. However, there was always a small gap between these blockages and the slot. Therefore, some source fluid would flow out the inner perforated tube, and then along the gap at each end of the slot. This would produce a very small flow of momentum toward the center of the slot that results in the small amount of necking at the ends seen in Figure 12.

The videos from each experiment were analyzed using MATLAB. The first few seconds of each video, taken before the plume was turned on, were time averaged to create a background image. Then the video was cropped into windows to the side of the plume that showed only clear ambient fluid and the dense lower layer. Each frame was then divided by the same window of the background image to correct for variations in the background light intensity. The background corrected windows were then horizontally averaged to create a vertical average light intensity for each frame. The interface at the first front was identified by finding the maximum vertical gradient in the light intensity for each frame. A sample contour plot of the concatenated horizontal averages along with the calculated interface height is shown in Figure 14. Some stray interface points are still shown in this image near the top at early times when the contrast across the interface was less sharp. These points were removed from the font position plots shown later.

Plots of the non-dimensional first front position for all experiments are shown in Figure 15. The linear-linear scale plot (top) shows that, as the nozzle width to tank depth decreases the first front position approaches the nozzle more rapidly as seen in Figure 7. The log-linear plot (bottom) shows the same behaviour but also highlights that for the widest nozzle (Experiments A and B with $W/H = 0.37$ and 0.35) the front position is very close to that of the pure line plume with no end entrainment (28), particularly at later times. At earlier times the front position is below that of the pure line plume solution indicating that there may be some entrainment through the ends of the plume further from the nozzle. For this nozzle width ($W = 19.4cm$, $W/H = 0.35 - 37$) the

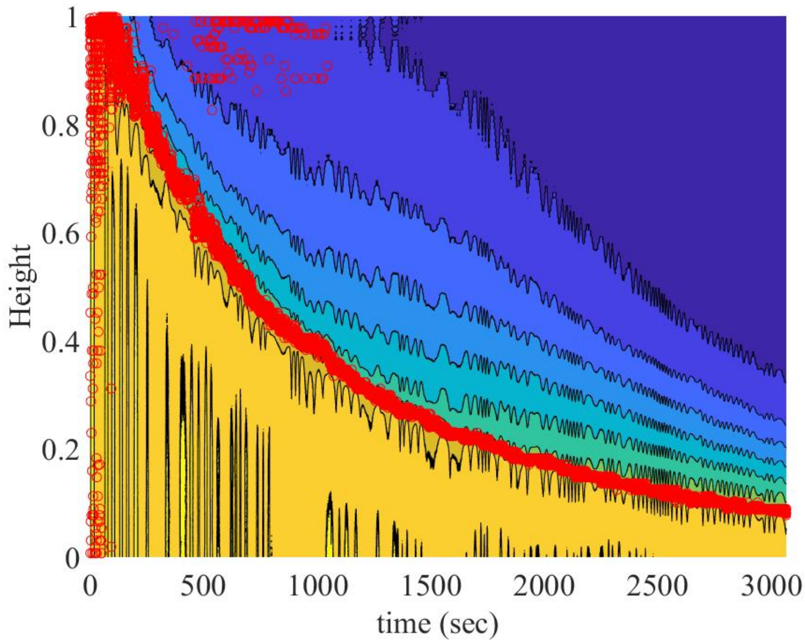

Fig. 14 Sample contour plot of light attenuation with the calculated interface height shown by red dots. Note that the vertical scale is the distance from the nozzle outlet scaled on the window height. This height was later corrected to be the depth of the tank below the nozzle outlet. The interface locations along the vertical axis and in the blue region above and to the right of the front were removed from the front position data set prior to comparison with the model.

height to nozzle width ratio is less than three suggesting that any transition occurs at or beyond $\lambda \approx 3$.

To further investigate the front position the data from experiment F (the narrowest nozzle) were plotted against the full model for a range of λ values and $\phi = 2$. The results are plotted in Figure 16. The model was run both with (right) and without (left) end entrainment. The front position from the model runs for $0.1 \leq \lambda \leq 10$ with no end entrainment consistently lay well above the experimental measurements suggesting that not including end entrainment leads to an under prediction of the actual plume volume flux at a given height. However, when end entrainment is included, the experimental data lies within the range of model predictions for $0.1 \leq \lambda \leq 10$. More specifically, the experimental measurements match closely the model for $\lambda = 3$. This value of λ is close to the prediction of the transition height based on the plume aspect ratio $2b/W = 1$ as discussed in §2.3.

It is interesting to note that $\phi = 2$ represents a reasonably short transition height with 75% of the transition occurring over a height of one nozzle width centered on $\lambda = 3$. This is consistent with the observations of Baines (1983) and Kaye and Linden (2004) for the merging of two round plumes. Both studies

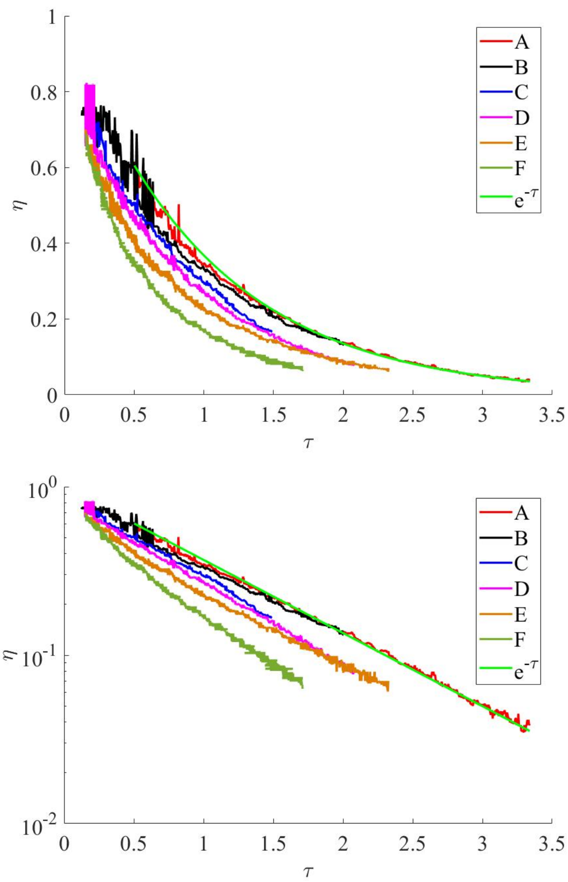

Fig. 15 Plots of non-dimensional front position (η) versus time (τ) for all 6 experiments on a linear vertical scale (top) and log vertical scale (bottom). Also shown is the analytic solution for a pure line plume ($\eta = e^{-\tau}$) in green.

observed that, once the two plumes made contact, there was a rapid change from dual plume to single plume behaviour over a distance similar to the plume thickness. All this suggests that, once the shape transition begins from a non-round plume geometry to a round plume geometry, the transition occurs over a height that scales on the plume's horizontal dimension. Intuitively this makes sense as the transition is a local phenomenon and, therefore, should scale on a local rather than global length scale. That said, the model predictions are not particularly sensitive to small changes in ϕ. The model predictions for the geometry of experiment F and different values of $0.5 \leq \phi \leq 5$ are shown in Figure 17. The difference in front position as a function of time with ϕ is within the experimental uncertainty. Therefore, it is not possible to determine the most appropriate value for ϕ. However, based on the results presented in Figure 16 the model values $\lambda = 3$ and $\phi = 2$ show good agreement.

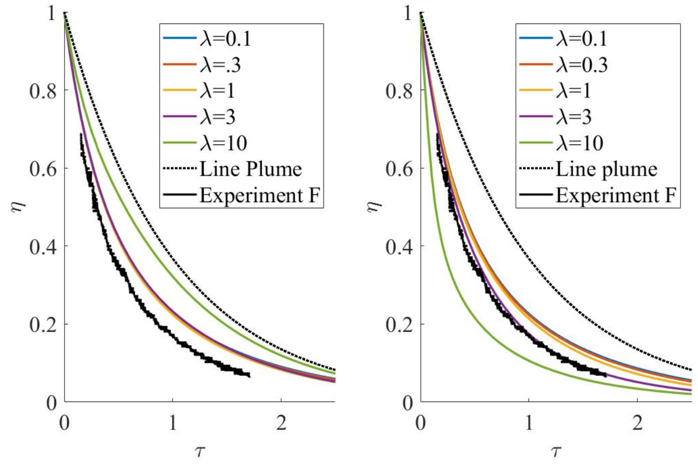

Fig. 16 Plots of non-dimensional front position (η) versus time (τ) for the narrowest nozzle (experiment F) and the model run for a range of λ values and $\phi = 2$. Also shown is the line plume analytic solution (black).

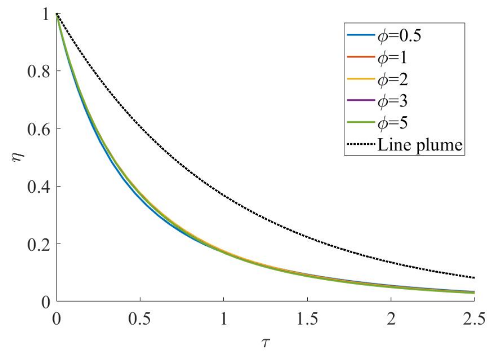

Fig. 17 Plots of non-dimensional front position (η) versus time (τ) for $\lambda = 3$ and different values of ϕ and for a line plume (black dashed line).

Based on these observations, the front position data from all six experiments were plotted against the model prediction for $\lambda = 3$, $\phi = 2$, and end entrainment turned on. These results are plotted in Figure 18. Note that in the early stages of each experiment there are large changes in the calculated front position, see in particular Figure 18(b). This is due to waves on the interface induced by the outflow interacting with the side walls of the container.

The agreement is generally very good except for Experiment A (top left) which matches the pure plume line for the entire height. In three of the tests (A, B, and E) the front position (η) deviates away from the model prediction toward the pure line plume result for small η. This might indicate that the rate of end entrainment decreases closer to the nozzle. However, the other three tests do not show this behaviour so no conclusions can be drawn on that point. Also shown on the plots is the transition height $\eta_T = \lambda W/H$ calculated for $\lambda = 3$. For experiments C-F there are experimental front position measurements on either side of the modeled transition height that agree well with the model developed herein.

5 Discussion and Conclusions

A model was presented for calculating the volume flux in a plume as it transitions from a line plume to a round plume. The model uses an entrainment formulation that can be applied to any plume cross section provided both the cross sectional area and entraining perimeter can be quantified. This approach reduces the transition problem to a geometric transition. The location of the geometric transition and the distance over which the transition is smoothed were implemented using the logistic equation with vertical distance scaled on the nozzle width.

When a transitioning line plume is placed in a filling box the non-dimensional front position (η) becomes a function of time, nozzle width to depth ratio, transition height λ, and the rate of transition ϕ. For a given nozzle width ratio W/H the rate of descent of the front increases with λ (Figure 6) whereas, when holding λ constant, the front descends more rapidly with decreasing W/H. The position of the front also depends on whether or not entrainment through the ends of the line plume is accounted for.

A series of line-plume filling box experiments were run to better understand this transition of a line plume to a round plume. Experiments were run for a broad range of nozzle width to box height ratios ($0.059 < W/H < 0.37$). In all cases the line plume nozzle was considerably narrower than the width of the box ($W/W_{box} \leq 0.17$). As such, there was no physical constraint preventing entrainment through the the ends of the line plume. Measurements of the front position well matched the model when entrainment through the plume ends was included in the model and the line-plume to round-plume transition was centered at $\lambda = Z_T/W = 3$ with $\phi = 2$. To the best of the authors' knowledge, this represents the first experimental measurements of a line plume that is open at the ends and is allowed to transition in to a round plume as it rises away from its source. The results of these experiments show that the simplest model of having a sharp transition from a pure line to a pure round plume with a virtual origin offset is overly simplified and inappropriate for modeling such a transition and that the round plume that forms above the transition height will be a forced plume.

While there is very good agreement between the experimental measurements of the front position and the model developed, there are still some unanswered questions that would point to future work. First,while the model agreement is best when end entrainment is included, observations of the plumes showed fairly vertical ends. Light could be shed on this problem with more precise measurements of the lateral concentration profile than were possible

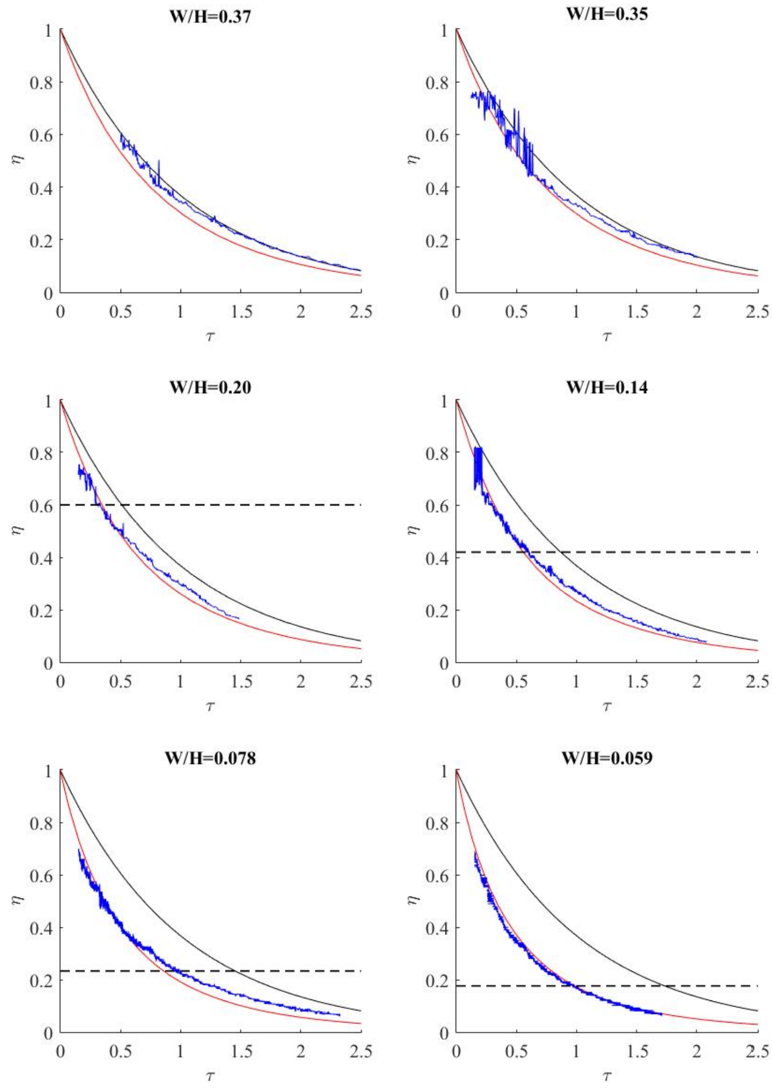

Fig. 18 Plots of non-dimensional front position (η) versus time (τ) for all 6 experiments (blue). Also shown are the line plume analytic solution (black) and the model run for $\lambda = 3$ and $\phi = 2$.

with the experimental setup available for this study. It would also be interesting to more directly measure the end mixing through measurements at the turbulent non-turbulent interface (TNTI) as done by Parker et al. (2019) for purely two dimensional line plumes. This approach could also elucidate the change in cross-sectional shape during the transition. Second, the model could also be improved by measurements of the entrianment coefficient through the ends of the line plume. In the model presented above the end entrainment coefficient was taken to be that of the rest of the line plume. While the actual entrainment coefficient will likely be of the same order as the pure line plume value, a more precise value could improve the model agreement. Finally, a alternate approach to transition the plume shape could be investigated. Herein, the shape transition is done using the hydraulic radius such that the actual shape is not determined at each step. It would be interesting to look at different models for the plume cross-sectional shape. This may include extending the modeling approach of Rooney (2015) to a finite length line plume.

Acknowledgements The authors would like to thank Dr. Abdul Khan for the use of the visualization tank for the experiments and Scott Black for assistance in the design and construction of the line plume nozzle. This material is based upon work supported by the National Science Foundation under Grant No.1703548. Any opinions, findings, and conclusions or recommendations expressed in the material are those of the author and do not necessarily reflect the views of the NSF.

References

Akhter R, Kaye NB (2020) Experimental investigation of a line plume in a filling box. Environmental Fluid Mechanics DOI 10.1007/s10652-020-09754-6

Albini FA (1996) Iterative solution of the radiation transport equations governing spread of fire in wildland fuel. Fizika Goreniya i Vzryva 32(5):71–82

Allgayer D, Hunt GR (2012) On the application of the light-attenuation technique as a tool for non-intrusive buoyancy measurements. Experimental Thermal and Fluid Science 38:257–261

Baines WD (1983) A technique for the direct measurement of volume flux of a plume. J Fluid Mech 132:247–256

Baines WD, Turner JS (1969) Turbulent buoyant convection from a source in a confined region. J Fluid Mech 37:51–80

Bejan A, Ziaei S, Lorente S (2014) Evolution: Why all plumes and jets evolve to round cross sections. Scientific Reports 4(1), DOI 10.1038/srep04730

Bush JWM, Woods AW (1999) Vortex generation by line plumes in a rotating stratified fluid. J Fluid Mech 388:289–313

Ching CY, Fernando HJS, Robles A (1995) Breakdown of line plumes in turbulent environments. Journal of Geophysical Research 100(C3):4707, DOI 10.1029/94jc02701

Ching CY, Fernando HJS, Mofor LA, Davies PA (1996) Interaction between multiple line plumes: a model study with applications to leads. J Phys Ocean 26:525–540

Fernando HJS, Ching CY (1993) Effects of background rotation on turbulent line plumes. Journal of Physical Oceanography 23(9):2125–2129, DOI 10.1175/1520-0485(1993)023¡2125:eobrot¿2.0.co;2

Hu L, Liu S, Zhang X (2017) Flame heights of line-source buoyant turbulent non-premixed jets withair entrainment constraint by two parallel side walls. Fuel 200:583–589

Hunt GR, Kaye NB (2005) Lazy plumes. J Fluid Mech 533:329–338

Huppert HE, Sparks RSJ, Whitehead JA, Hallworth MA (1986) Replenishment of magma chambers by light inputs. J Geophys Res 91:6113–6122

Jackson RH, Shroyer EL, Nash JD, Sutherland DA, Carroll D, Fried MJ, Catania GA, Bartholomaus TC, Stearns LA (2017) Near-glacier surveying of a subglacial discharge plume: Implications for plume parameterizations. Geophysical Research Letters 44(13):6886–6894, DOI 10.1002/2017gl073602

Kaye NB, Hunt GR (2007) Overturning in a filling box. J Fluid Mech 576:297–323

Kaye NB, Linden PF (2004) Coalescing axisymmetric turbulent plumes. J Fluid Mech 502:41–63

Kotsovinos NE (1977) Plane turbulent buoyant jets. part 2. turbulence structure. J Fluid Mech 81:45–62

Kotsovinos NE, List EJ (1977) Plane turbulent buoyant jets. part 1. integral properties. J Fluid Mech 81:25–44

Lee JHW, Chu VH (2003) Turbulent jets and plumes a Lagrangian approach. Kluwer Academic Publishers

Lee SL, Emmons HW (1961) A study of natural convection above a line fire. Journal of Fluid Mechanics 11(03):353, DOI 10.1017/s0022112061000573

Li S, Flynn MR (2020a) Merging of long rows of plumes: Crosswinds, multiple rows, and applications to cooling towers. Physical Review Fluids 5(9):094,502, DOI 10.1103/physrevfluids.5.094502

Li S, Flynn MR (2020b) Merging of two plumes from area sources with applications to cooling towers. Phys Rev Fluids 5:054,502, DOI 10.1103/PhysRevFluids.5.054502

Linden PF, Lane-Serff GF, Smeed DA (1990) Emptying filling boxes, the fluid mechanics of natural ventilation. J Fluid Mech 212:309–335

Ma Y, Flynn MR, Sutherland BR (2017) Convection from a line-source into a two-layer stratified ambient fluid. Journal of Fluid Mechanics 818:46–67, DOI 10.1017/jfm.2017.143

Morton BR, Middleton J (1973) Scale diagrams for forced plumes. J Fluid Mech 58:165–176

Morton BR, Taylor GI, Turner JS (1956) Turbulent gravitational convection from maintained and instantaneous sources. Proc Roy Soc Lond A 234:1–23

Paillat S, Kaminski E (2014) Entrainment in plane turbulent pure plumes. Journal of Fluid Mechanics 755, DOI 10.1017/jfm.2014.424

Parker DA, Burridge HC, Partridge JL, Linden PF (2019) A comparison of entrainment in turbulent line plumes adjacent to and distant from a vertical wall. Journal of Fluid Mechanics 882, DOI 10.1017/jfm.2019.790

Ramaprian BR, Chandrasekhara MS (1989) Measurements in vertical plane turbulent plumes. Journal of Fluids Engineering 111(1):69–77, DOI 10.1115/1.3243602

Roberts PJW (1979) Line plume and ocean outfall dispersion. Journal of the Hydraulics Division 105(4):313–331, DOI 10.1061/jyceaj.0005175

Rooney GG (2015) Merging of a row of plumes or jets with an application to plume rise in a channel. J Fluid Mech 771

Rooney GG (2016) Merging of two or more plumes arranged around a circle. Journal of Fluid Mechanics 796:712–731

Thomas P (1987) On the upward movement of smoke and related shopping mall problems. Fire Safety Journal 12(3):191–203, DOI 10.1016/0379-7112(87)90005-1

Thomas P, Morgan H, Marshall N (1998) The spill plume in smoke control design. Fire Safety Journal 30(1):21–46, DOI 10.1016/s0379-7112(97)00037-4